Journal of Alloys and Compounds 655 (2016) 442–447

Contents lists available at ScienceDirect

Journal of Alloys and Compounds

journal homepage: http://www.elsevier.com/locate/jalcom

Terahertz conductivities of VO_2 thin films grown under different sputtering gas pressures

Y.Y. Luo [a, *], F.H. Su [a, **], S.S. Pan [a], S.C. Xu [a], C. Zhang [a], J. Pan [a], J.M. Dai [a], P. Li [b], G.H. Li [a, c, ***]

[a] Key Laboratory of Materials Physics, Anhui Key Laboratory of Nanomaterials and Nanostructures, Institute of Solid State Physics, Chinese Academy of Sciences, Hefei 230031, PR China
[b] High Magnetic Field Laboratory, Chinese Academy of Science, Hefei, 230031 Anhui, PR China
[c] School of Chemistry and Materials Science, University of Science and Technology of China, Hefei 230026, PR China

ARTICLE INFO

Article history:
Received 18 June 2015
Received in revised form
29 July 2015
Accepted 29 August 2015
Available online 8 September 2015

Keywords:
Vanadium dioxide
Terahertz
Metal-insulator transition
Drude-Smith model
Effective medium theory

ABSTRACT

The terahertz (THz) conductivities in the metal-insulator transition process of VO_2 thin films on quartz substrates were investigated by using terahertz time-domain spectroscopy. It was found that the THz absorption and conductivity of the thin films are sensitive to the sputtering gas pressure, and the maximum THz amplitude modulation can reach as high as 75.9%. The complex THz conductivity in metallic state of the thin films can be well-fitted by the Drude-Smith model, and the temperature-dependent metallic domain fractions can be extracted by effective medium theory simulation. Based on these results, the metal-insulator transition of the VO_2 thin films can be characterized. The mechanisms of the THz transmission and conductivity were analyzed and discussed.

1. Introduction

Monoclinic vanadium dioxide (VO_2) is an attractive near-room temperature thermochromic material because of its remarkable change in optical and electronic properties during the reversible metal-insulator transition (MIT) [1–3], and can be potentially used in many areas, such as optical memory devices [4] and optic-electric switches devices [5,6]. Great progress has been made in the growth of high-quality VO_2 material [7–9], phase transition mechanism [10,11] and optimization of the thermochromic property [12–15] over the past few decades. The research on the basic interactions between VO_2 and electromagnetic wave in the terahertz ranges has attracted extensive attentions in recent years [16]. Especially, the coherent detection of the broadband THz pulse permits the direct access to the complex THz conductivity and dynamic metal-insulator transition by THz spectroscopy [11,17–20], providing an alternative to understanding the fundamental physical mechanism in strongly correlated systems. It has been demonstrated that the VO_2 thin films can behave as a tunable coating to support the active THz metamaterials [21,22], such as tunable polarizer, filter, switch and modulator with considerable dynamic range and multiple modulation ways, which can help us to develop some novel optics devices in the THz gap. In comparison with bulk crystal, the optical and electrical properties of the VO_2 thin film will be affected not only by the morphology but also by the complex interactions between strain field originating from the intergrain interaction and the substrate-film boundary as well [23]. And therefore, considerable efforts have been dedicated to regulate the morphology, grain size, crystal quality and thickness of VO_2 thin film by different growth conditions [24], substrate types [25,26] and substrate orientations [7,27]. Such methods make it possible optimize the modulation depth, the insertion loss and dynamic range in THz spectrum range. Different growth methods like sol–gel [10,28], solution-based process [29], thermolysis [30], pulsed laser deposition [31,32] and sputtering [12,26] have been explored to grow stoichiometric VO_2 thin film. Among them, the reactive

* Corresponding author.
** Corresponding author.
*** Corresponding author. Key Laboratory of Materials Physics, Anhui Key Laboratory of Nanomaterials and Nanostructures, Institute of Solid State Physics, Chinese Academy of Sciences, Hefei 230031, PR China.
E-mail addresses: yyluo@issp.ac.cn (Y.Y. Luo), fhsu@issp.ac.cn (F.H. Su), ghli@issp.ac.cn (G.H. Li).

http://dx.doi.org/10.1016/j.jallcom.2015.08.254
0925-8388/

sputtering technique is widely used method to grow VO_2 thin film with excellent crystal quality due to the diversiform controlling parameters like O_2 flow ratio, sputtering power and sputtering gas pressure that can normally control the stoichiometry, microstructure and crystal quality of the as-grown thin film. In previous work, we have studied the optical switching properties of VO_2 thin films by infrared (IR) spectrum [33], and it was found that the external growth factors like sputtering gas pressure and O_2 flow ratio can be employed to tailor the phase transition temperature, hysteresis width and the amplitude of the transition in IR range. In THz spectra region, the fundamental correlations between the THz conductivity and film growth parameters in reactive sputtering process that is essential to develop tunable VO_2 based THz device and understand the phase transition remain rarely explored. In this paper, we report the THz (0.2–1.3 THz) transmission and conductivity of the VO_2 thin films grown under different sputtering gas pressures. It was found that the complex terahertz conductivities of the VO_2 thin films in the metal-insulator transition process can be turned by growth parameters, and from which the metal-insulator transition of the VO_2 thin films can be well-characterized.

2. Experimental section

The VO_2 thin films were deposited on quartz substrate by radio frequency reactive magnetron sputtering. Our previous study found that the pure VO_2 thin films can be obtained only at the gas pressure of 0.2–0.4 Pa [33], and therefore, the VO_2 thin films used in this study were grown under the conditions of 0.2–0.4 Pa sputtering gas pressures, 3.5% of O_2 flow ratio, and 350 W of sputtering power. The film thickness is found to be about 350, 400, and 370 nm at the sputtering gas pressure of 0.2, 0.3, and 0.4 Pa, respectively. THz time-domain spectroscopy (TDS) was performed by using a standard transmission configuration, in which a mode-locked Ti:sapphire laser deliver the pulses with duration of 100 fs, center wavelength of 800 nm, and repetition rate of 76 MHz, which are divided into pump and probe beam. The pumping laser pulses are focused on LT-GaAs photoconductive antenna and generate the broadband THz pulse. The free-space electro-optic sampling technique via ZnTe crystal is employed to detect the electric field amplitude of the THz waveforms in time domain. The fast Fourier transformation (FFT) for the THz waveform is carried out to obtain the THz spectrum in frequency domain. The TDS measurements were undertaken under a dry nitrogen purge. The measuring temperature of the heater module lies in the range of 20–300 °C with the temperature accuracy of 1 K.

3. Results and discussion

Fig. 1 shows the XRD patterns of the as-grown thin films on the quartz substrate at different sputtering gas pressures. One can see that the diffraction peaks of the thin films at all sputtering gas pressures match well with monoclinic VO_2 (JCPDS card no. 01-072-0514), and a solo strong diffraction peak at $2\theta = 27.88^\circ$ indicates that the VO_2 thin films are of [011] preferred orientation. The grain size can be estimated from XRD pattern using the Scherrer's formula [34]: $D = \frac{0.9\lambda}{\beta\cos\theta}$, where β is the full width at half maximum of a diffraction peak at 2θ corrected for instrumental broadening, and the corresponding arithmetic mean grain size of VO_2 based on the first four strong diffraction peaks is about 139.9, 123.9, and 108.9 nm at sputtering gas pressure of 0.2, 0.3 and 0.4 Pa, respectively (see Table 1). Obviously, the average grain size of the thin films decreases with increasing sputtering gas pressure. In the sputtering process, it is easy to generate the high-energy electrons and ions due to the less collision as the gas pressure decreases, which help to increase the energy of sputtered atom and the thermal effect of the substrate. The two factors can promote the growth of crystalline and increase the grain size. In addition, the crystallinity of the thin films was determined by the FWHM of the first four strong diffraction peaks, and normally, the lower the FWHM value the higher the crystallinity of the thin films [35]. Table 1 shows the FWHM value of the VO_2 thin films grown in 0.3 Pa is lowest compared with that of other samples, which demonstrates the VO_2 thin films grown in 0.3 Pa has high crystallinity. Fig. 2 shows typical FESEM images of the thin films grown at different sputtering gas pressures. One can see that the as-grown thin films are composed of random arrayed columnar particles. The particle size is larger than the mean grain size obtained by XRD analysis.

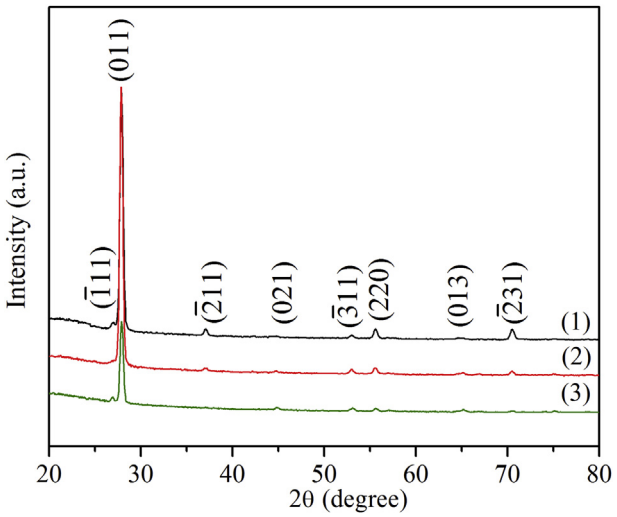

Fig. 1. XRD patterns of VO_2 thin films grown under sputtering gas pressure of (1) 0.2, (2) 0.3, and (3) 0.4 Pa.

Table 1
Some parameters calculated according to Scherrer's formula.

No.	(hkl)	FWHM	Grain Size	Avreage grain size (nm)
0.2 Pa	(011)	0.398	143.6	139.9
	(2̄11)	0.44	164.3	
	(3̄11)	0.49	125	
	(220)	0.43	126.5	
0.3 Pa	(011)	0.384	233.8	123.9
	(2̄11)	0.45	83	
	(3̄11)	0.46	80	
	(220)	0.44	98.7	
0.4 Pa	(011)	0.398	167.1	108.9
	(021)	0.44	94.4	
	(3̄11)	0.49	63	
	(220)	0.43	110.9	

The transmitted THz pulse waveforms of the VO_2 thin films were measured at temperature range from 30 to 85 °C with the THz transmissions through the bare quartz substrates as references. It was found that all the VO_2 thin films at semiconductor-phase are highly transparent in the studied spectrum range. Fig. 3 shows the transmitted THz electric filed pulses through VO_2 thin films at temperature of 30 °C and 85 °C, corresponding respectively to semiconductor- and metal-phase VO_2. One can see that the THz transmission amplitude decreases pronouncedly after transition from semiconductor phase to metal phase. The THz modulation depth (calculated from the equation: $\Delta A = (A_i - A_m)/A_i$, where A_m and A_i are the THz field amplitudes at metal and insulating phase, respectively), is about 75.9, 72.1 and 60.5% for the VO_2 thin films at

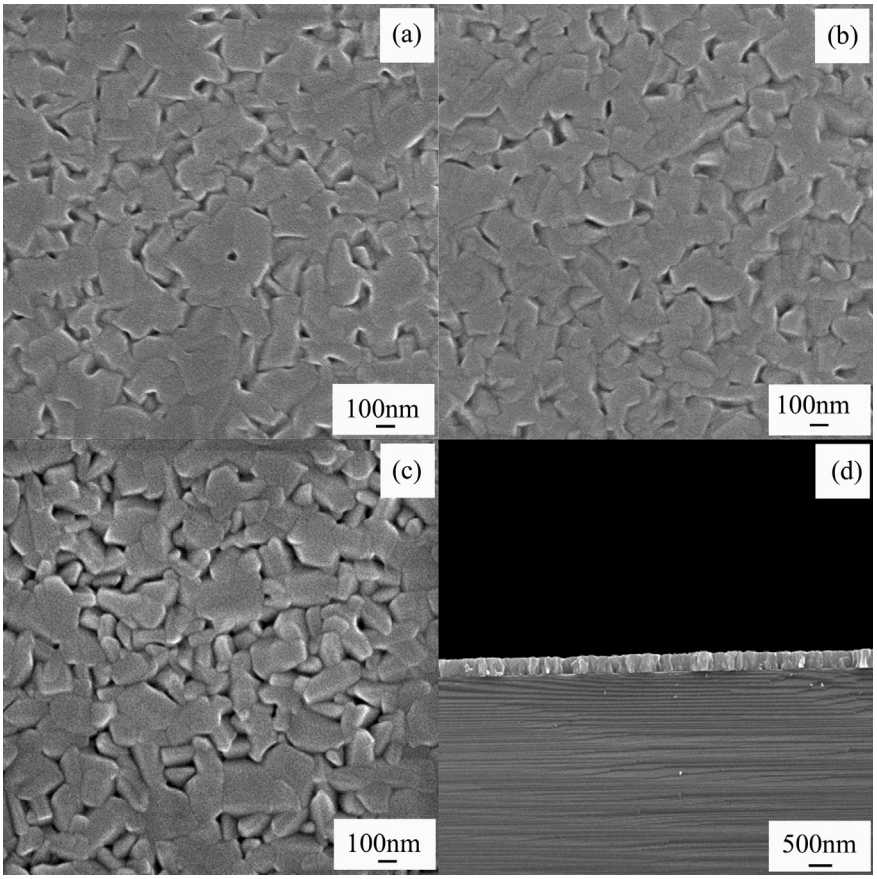

Fig. 2. FESEM images of as-deposited VO_2 thin films at sputtering gas pressure of (a) 0.2, (b) 0.3, and (c) 0.4 Pa (d) Cross-sectional FESEM image of (b).

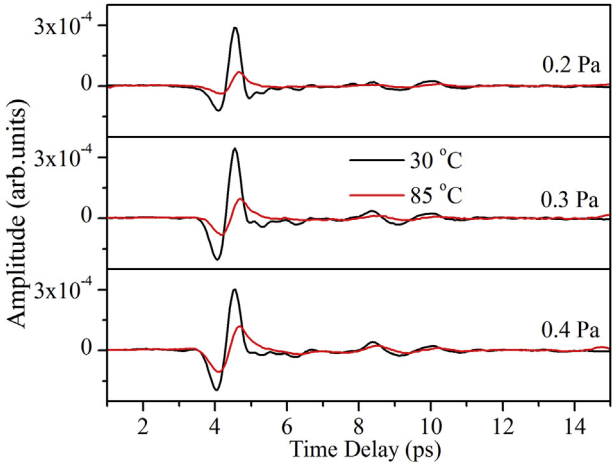

Fig. 3. Transmitted THz waveforms through the VO_2 thin films on quartz substrate grown under different sputtering gas pressures before and after metal-insulator transition.

sputtering gas pressure of 0.2, 0.3, and 0.4 Pa, respectively. The maximum modulation depth is comparable with the reported value for the VO_2 film deposited on the c-sapphire substrate [26].

For a thin conducting layer on the dielectric substrate, the complex THz conductivity, $\tilde{\sigma}(\omega) = \sigma_1(\omega) + i\sigma_2(\omega)$, can be determined by the THz electric-field amplitude transmission normalized to the bared substrate according to the following equation [36].

$$\frac{\tilde{E}_{f+s(\omega)}}{\tilde{E}_{s(\omega)}} = \frac{1+n_s}{1+n_s+z_0\tilde{\sigma}(\omega)t_f} \quad (1)$$

where $\frac{\tilde{E}_{f+s(\omega)}}{\tilde{E}_{s(\omega)}}$ is the THz electric-field amplitude transmission of the thin film normalized to the bared substrate, n_s is a nearly frequency-independent index of refraction of quartz substrate, $z_0 = 377\ \Omega$ the impedance of free space, t_f the thickness of the VO_2 thin film. The obtained complex conductivity spectra in frequency domain of the VO_2 thin films at 85 °C are shown in Fig. 4, demonstrating that the σ_1 increases while the σ_2 decreases with increasing frequency. The defects content in thin films is generally higher than that in bulk [36], and therefore the carrier localization and/or trapping will result in a negative σ_2.

The Drude-Smith model [36,37] can be used to describe the complex THz conductivity of VO_2 thin films in metallic state by considering the backscattering and localization of carriers:

$$\sigma_{DS}(\omega) = \frac{n\,e^2\,\tau_{DS}}{m^*(1-i\omega\tau_{DS})}\left(1+\frac{c_1}{1-i\omega\tau_{DS}}\right) \quad (2)$$

where the parameter c_1 denotes the fraction of the initial velocity of the electron that is retained after a scattering event. The n and τ_{DS} are respectively the electron density and scattering time, $m^* = 2m_e$ the effective mass of electron in VO_2 and the e electric charge. The fitting results are shown in Fig. 4, which clearly demonstrates that the THz complex conductivities in metal-phase VO_2 thin films are consistent with the Drude-Smith model. The obtained scattering time from the best fitting for the three thin films is all about 22 fs, while the c_1 factor is about −0.95, −0.97, −0.98 for the VO_2 thin film

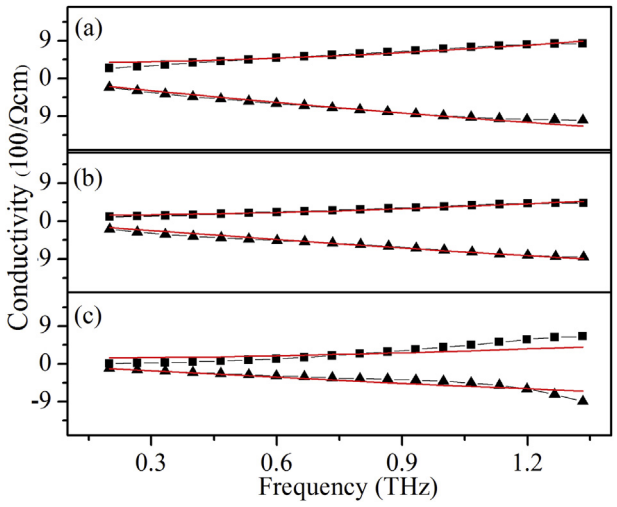

Fig. 4. Real (square) and imaginary (triangle) parts of THz conductivity of VO_2 thin films grown under sputtering gas pressure of (a) 0.2, (b) 0.3 and (c) 0.4 Pa measured at 85 °C. The solid red lines are fitting curves from Drude-Smith model. (For interpretation of the references to color in this figure caption, the reader is referred to the web version of this article.)

grown under sputtering pressure of 0.2, 0.3, and 0.4 Pa, respectively. It is worth noting that the absolute value of c_1 slightly increases with increasing sputtering pressure. The c_1 value close to −1 indicates that a strong carrier backscattering and localization may dominate in the electron transport in THz frequency range. Our XRD analysis shown that the higher the sputtering pressure the smaller the grain size. A smaller grain will lead to a stronger backscattering [38], and therefore, the sputtering pressure dependence of the c_1 factor can be attributed to the various morphology of the VO_2 thin films. It should be mentioned that the c_1 value obtained in present study is larger than that reported in literature [37,38], where they found that the backscattering effect is negligible when the grain size is larger than 100 nm. In fact, there is no satisfactory argument for the microscopic mechanism of the backscattering characterized by c_1 value in this Drude-Smith model. K. Shimakawa et al. proposed a tunneling model illustrating the electron scattering process between adjacent grains [39], in which both grain size and grain boundaries determine the electron scattering. In this model, the electron tunneling through grain boundaries is also associated with the backscattering term in Drude-smith model. Our experimental results agree with Drude-Smith model with large c_1 factor, which may indicate that the tunneling possibility through grain boundaries in our samples is much smaller than that in Refs. [37,38]. This electron tunneling effect is related to the factors like film microstructure, defects, crystal quality and substrate. The total electron density determined from Drude-Smith model is about 2.6×10^{21}, 1.92×10^{21} and 1.3×10^{21} cm^{-3} for the VO_2 thin film grown under sputtering pressure of 0.2, 0.3, and 0.4 Pa, respectively, which are in a reasonable range compared with the measured electron density ($2–3 \times 10^{21}$ cm^{-3}) by THz spectra in VO_2 films [40]. The electron density of the VO_2 thin film decreases obviously with increasing the sputtering gas pressure, which will affect its THz conductivity and transmission behavior. The VO_2 thin film grown at 0.2 Pa has a largest grain size in present study, and thus has the least number of grain boundaries compared with the other two thin films. As a result, most electrons in metallic domain are mobile and contribute to a higher THz conductivities and a lower THz transmission in the metallic state. Therefore, the VO_2 thin film grown at 0.2 Pa has the highest electron density and THz modulation depth.

The semiconducting and metallic domains will coexist in the VO_2 thin film near the metal-insulator transition temperature. This spatial heterogeneity in the VO_2 thin film will strongly affect its effective dielectric property. It is known that the macroscopic dielectric constant of VO_2 in the phase transition process can be modeled by the effective medium theory (EMT), which represents a kind of mean field description for inhomogeneous media. Maxwell-Garnett equation can be employed for the simulation [41]:

$$\frac{\varepsilon^* - \varepsilon_i}{\varepsilon^* + 2\varepsilon_i} = f\frac{\varepsilon_m - \varepsilon_i}{\varepsilon_m + 2\varepsilon_i}, \tag{3}$$

where, ε_m and ε_i are respectively the dielectric constant in the metallic and insulating phase, f the volume fraction of metallic phase. The $\tilde{\varepsilon}$ is related to the THz conductivity through the equation:

$$\tilde{\varepsilon}(\omega) = \varepsilon_\infty + i\frac{\tilde{\sigma}(\omega)}{\omega\varepsilon_0} \tag{4}$$

where ε_∞ is the dielectric constant at high frequencies and ε_0 is the vacuum dielectric constant.

Fig. 5 show the fitting results of the THz conductivity from EMT model at several temperatures for the VO_2 thin films grown at 0.3 Pa (solid red lines). At each temperature, the parameters n, τ_{DS}, and c_1 were obtained by self-consistently fitting $\sigma_1(\omega)$ and $\sigma_2(\omega)$. From Fig. 5 one can clearly see that the THz conductivity spectrum can be well-fitted by the EMT, in which the parameter c_1 is nearly to −1 and is temperature-independent across the MIT, suggesting that the VO_2 grains are either entirely insulating or metallic. The carrier density of the VO_2 thin film increases from about 6.65×10^{19} cm^{-3} at 60 °C to 1.91×10^{21} cm^{-3} at 80 °C.

The volume fraction of the metallic domains (f) can be obtained from the best fitting and the results are shown in Fig. 6. One can see that with increasing temperature the f value increases from zero in semiconductor state to one at metal state, and the vice versa, resulting in a hysteresis loop. The hysteresis loop can be well described by Boltzmann function [37]:

$$f(\mathrm{T}) = f_{\max}\left(1 - \frac{1}{1 + \exp[(T - T_0)/\Delta T)]}\right) \tag{5}$$

where $f_{\max}$ is the volume fraction of the metallic domain at 85 °C,

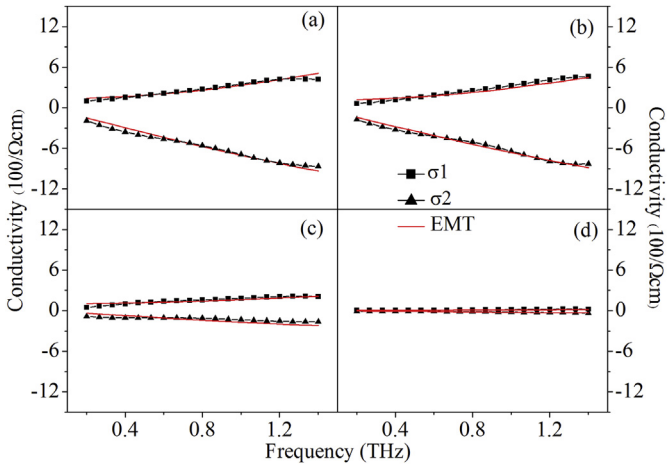

Fig. 5. Real (squares) and imaginary (triangles) components of the THz conductivity measured at (a) 80, (b) 70, (c) 65 and (d) 60 °C of VO_2 thin film grown at 0.3 Pa. The solid red lines are fitting curves from EMT model. (For interpretation of the references to color in this figure caption, the reader is referred to the web version of this article.)

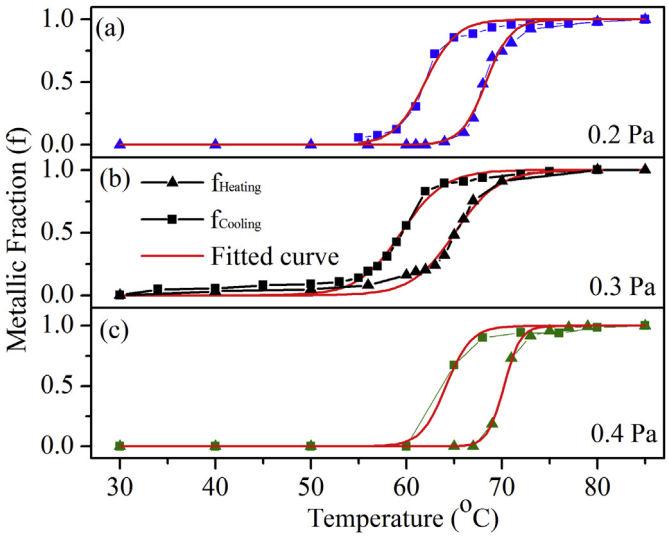

Fig. 6. Volume fraction of metallic domain in heating (triangle) and cooling (square) cycles. The solid red lines are fitting curves from the Boltzmann function (For interpretation of the references to color in this figure caption, the reader is referred to the web version of this article.)

which is set to 1 for the fitting. From Equ. (5), we can calculate the transition temperature of the VO_2 thin film in the heating/cooling cycle, which is 68.3/61.9, 65.1/59.5, and 70.2/64.1 °C for the VO_2 thin film grown under sputtering gas pressure of 0.2, 0.3 and 0.4 Pa, respectively. It can be seen that the thin film grown under sputtering gas pressure of 0.3 Pa has the lowest phase transition temperature and hysteresis width in comparison with other two samples. It is worth note that the hysteresis width obtained from THz-TDS is lower compared to the results of the infrared spectroscopy [33], due to the different measuring environments. The width and shape of the hysteresis cycle are primarily determined by the competition between the crystallinity and grain size as demonstrated in Refs. [35,42]. In addition, the intrinsic stress and defects also affects the phase transition temperature of VO_2 (M) films, the larger the intrinsic stress, the higher the transition temperature. Being having the lowest intrinsic stress, the VO_2 (M) sample grown at 0.3 Pa thus has the lowest transition temperature as compared with other two samples.

4. Conclusion

In summary, we have investigated the optical conductivities of VO_2 thin films using terahertz time-domain spectroscopy. It was found that the sputtering gas pressures in the growth of the thin films affect their THz transmission and conductivity because the grain size in VO_2 thin film is sputtering gas pressure-dependent. The terahertz conductivity of the VO_2 thin film in metallic state can be well-fitted by Drude-Smith model. The fitting results revealed that the electron density decreases with increasing the sputtering gas pressure and the carrier backscattering plays a key role in the electron transport of VO_2 in THz region. The hysteresis loop can be obtained by the plot of metallic volume fraction by the EMT simulation from the temperature-dependent THz conductivity. The phase transition temperature can be obtained by fitting the Boltzmann function, and the variation trend of the phase transition temperature is in consistency with our previous results obtained by IR transmission spectroscopy. Our results not only provide that the THz transmission and conductivity of the VO_2 thin films can be regulated by growth conditions, but demonstrate that the terahertz time-domain spectroscopy is an effective tool to understand the metal-insulator transition of the VO_2 thin films.

Acknowledgments

This work was financially supported by the National Natural Science Foundation of China (Grant Nos. 51372250, 11004199, 11104270 and 51471163).

References

[1] C.Z. Wu, F. Feng, Y. Xie, Chem. Soc. Rev. 42 (12) (2013) 5157.
[2] J.D. Zhou, Y.F. Gao, Z.T. Zhang, H.J. Luo, C.X. Cao, Z. Chen, L. Dai, X.L. Liu, Sci. Rep. 3 (2013) 3029.
[3] A. Gentle, A.I. Maaroof, G.B. Smith, Nanotechnology 18 (2) (2007) 025202.
[4] H. Coy, R. Cabrera, N. Sepulveda, F.E. Fernandez, J. Appl. Phys. 108 (11) (2010) 113115.
[5] H.T. Kim, B.J. Kim, S. Choi, B.G. Chae, Y.W. Lee, T. Driscoll, M.M. Qazilbash, D.N. Basov, J. Appl. Phys. 107 (2) (2010) 023702.
[6] H. Yada, T. Miyamoto, H. Okamoto, Appl. Phys. Lett. 102 (2013) 091104.
[7] T.-H. Yang, R. Aggarwal, A. Gupta, H.H. Zhou, R.J. Narayan, J. Narayan, J. Appl. Phys. 107 (5) (2010) 053514.
[8] W.W. Li, Q. Yu, J.R. Liang, K. Jiang, Z.G. Hu, J. Liu, H.D. Chen, J.H. Chu, Appl. Phys. Lett. 99 (24) (2011) 241903.
[9] M. Li, X. Wu, L. Li, Y. Wang, D. Li, J. Pan, S. Li, L. Sun, G. Li, J. Mater. Chem. A 2 (13) (2014) 4520.
[10] H.-T. Kim, Y.W. Lee, B.-J. Kim, B.-G. Chae, S.J. Yun, K.-Y. Kang, K.-J. Han, K.-J. Yee, Y.-S. Lim, Phys. Rev. Lett. 97 (2006) 266401.
[11] M.M. Qazilbash, A.A. Schafgans, K.S. Burch, S.J. Yun, B.G. Chae, B.J. Kim, H.T. Kim, D.N. Basov, Phys. Rev. B 77 (11) (2008) 115121.
[12] B. Viswanath, C. Ko, Z. Yang, S. Ramanathan, J. Appl. Phys. 109 (6) (2011) 063512.
[13] R. Lopez, L.A. Boatner, T.E. Haynes, R.F. Haglund Jr., L.C. Feldman, Appl. Phys. Lett. 79 (19) (2001) 3161.
[14] S.Y. Li, G.A. Niklasson, C.G. Granqvist, J. Appl. Phys. 108 (2010) 063525.
[15] D. Li, M. Li, J. Pan, Y. Luo, H. Wu, Y. Zhang, G. Li, ACS Appl. Mater. Interfaces 6 (9) (2014) 6555.
[16] T.L. Cocker, L.V. Titova, S. Fourmaux, G. Holloway, H.-C. Bandulet, D. Brassard, J.-C. Kieffer, M.A. El Khakani, F.A. Hegmann, Phys. Rev. B 85 (2012) 155120.
[17] J.M. Laforge, T.L. Cocker, A.L. Beaudry, K. Cui, R.T. Tucker, M.T. Taschuk, F.A. Hegmann, M.J. Brett, Nanotechnology 25 (3) (2014) 035701.
[18] Y. Kawano, Nanotechnology 24 (21) (2013) 214004.
[19] C. Kübler, H. Ehrke, R. Huber, R. Lopez, A. Halabica, R. Haglund, A. Leitenstorfer, Phys. Rev. Lett. 99 (11) (2007) 116401.
[20] M. Walther, D. Cooke, C. Sherstan, M. Hajar, M. Freeman, F. Hegmann, Phys. Rev. B 76 (12) (2007) 125408.
[21] M.K. Liu, H.Y. Hwang, H. Tao, A.C. Strikwerda, K. Fan, G.R. Keiser, A.J. Sternbach, K.G. West, S. Kittiwatanakul, J.W. Lu, S.A. Wolf, F.G. Omenetto, X. Zhang, K.A. Nelson, R.D. Averitt, Nature 487 (7407) (2012) 345.
[22] M. Seo, J. Kyoung, H. Park, S. Koo, H.S. Kim, H. Bernien, B.J. Kim, J.H. Choe, Y.H. Ahn, H.T. Kim, N. Park, Q.H. Park, K. Ahn, D.S. Kim, Nano Lett. 10 (6) (2010) 2064.
[23] J.I. Sohn, H.J. Joo, K.S. Kim, H.W. Yang, A.R. Jang, D. Ahn, H.H. Lee, S. Cha, D.J. Kang, J.M. Kim, M.E. Welland, Nanotechnology 23 (20) (2012) 205707.
[24] Y. Zhao, C.H. Chen, X. Pan, Y.H. Zhu, M. Holtz, A. Bernussi, Z.Y. Fan, J. Appl. Phys. 114 (11) (2013) 113509.
[25] Q.W. Shi, W.X. Huang, J. Wu, Y.X. Zhang, Y.J. Xu, Y. Zhang, S. Qiao, J.Z. Yan, J. Appl. Phys. 112 (2012) 033523.
[26] Y. Zhao, J. Hwan Lee, Y.H. Zhu, M. Nazari, C.H. Chen, H.Y. Wang, A. Bernussi, M. Holtz, Z.Y. Fan, J. Appl. Phys. 111 (5) (2012) 053533.
[27] Y.H. Zhu, Y. Zhao, M. Holtz, Z.Y. Fan, A.A. Bernussi, J. Opt. Soc. Am. B 29 (9) (2012) 2373.
[28] Q.W. Shi, W.X. Huang, T.C. Lu, Y.X. Zhang, F. Yue, S. Qiao, Y. Xiao, Appl. Phys. Lett. 104 (7) (2014) 071903.
[29] Q.W. Shi, W.X. Huang, Y.J. Xu, Y.X. Zhang, F. Yue, S. Qiao, S.P. Zheng, J.Z. Yan, J. Phys. D Appl. Phys. 45 (38) (2012) 385302.
[30] F.Y. Kong, M. Li, S.S. Pan, Y.X. Zhang, G.H. Li, Mater. Res. Bull. 46 (11) (2011) 2100.
[31] D.Y. Fu, K. Liu, T. Tao, K. Lo, C. Cheng, B. Liu, R. Zhang, H.A. Bechtel, J.Q. Wu, J. Appl. Phys. 113 (2013) 043707.
[32] H.W. Liu, L.M. Wong, S.J. Wang, S.H. Tang, X.H. Zhang, Appl. Phys. Lett. 103 (15) (2013) 151908.
[33] Y.Y. Luo, L.Q. Zhu, Y.X. Zhang, S.S. Pan, S.C. Xu, M. Liu, G.H. Li, J. Appl. Phys. 113 (18) (2013) 183520.
[34] C. Liu, F. Shang, G. Pan, F. Wang, Z. Zhou, W. Gong, Z. Zi, Y. Wei, X. Chen, J. Lv, G. He, M. Zhang, X. Song, Z. Sun, Appl. Surf. Sci. 305 (2014) 753–759.
[35] J.Y. Suh, R. Lopez, L.C. Feldman, R.F. Haglund, J. Appl. Phys. 96 (2) (2004) 1209.
[36] T.L. Cocker, L.V. Titova, S. Fourmaux, H.C. Bandulet, D. Brassard, J.C. Kieffer, M.A. El Khakani, F.A. Hegmann, Appl. Phys. Lett. 97 (22) (2010) 221905.
[37] P.U. Jepsen, B.M. Fischer, A. Thoman, H. Helm, J.Y. Suh, R. Lopez, R.F. Haglund Jr., Phys. Rev. B 74 (2006) 205103.

[38] D.G. Cooke, A.N. MacDonald, A. Hryciw, J. Wang, Q. Li, A. Meldrum, F.A. Hegmann, Phys. Rev. B 73 (19) (2006) 193311.
[39] K. Shimakawa, T. Itoh, H. Naito, S.O. Kasap, Appl. Phys. Lett. 100 (13) (2012) 132102.
[40] H.S. Choi, J.S. Ahn, J.H. Jung, T.W. Noh, D.H. Kim, Phys. Rev. B 54 (7) (1996) 4621.
[41] J. Lloyd-Hughes, T.I. Jeon, J. Infrared Millim. Terahertz Waves 33 (9) (2012) 871.
[42] Y. Xiong, Q.-Y. Wen, Z. Chen, W. Tian, T.-L. Wen, Y.-L. Jing, Q.-H. Yang, H.-W. Zhang, J. Phys. D Appl. Phys. 47 (45) (2014) 455304.